A compact, ultra-high vacuum ion source for isotopically enriching and depositing ^{28}Si thin films

K. Tang,[1,3] H. S. Kim,[2,3] A. R. Ramanayaka[3], D. S. Simons[3], and J. M. Pomeroy[3,*]
[1]*Department of Materials Science and Engineering, University of Maryland, College Park, Maryland 20740, USA*
[2]*Department of Electrical and Computer Engineering, University of Maryland, College Park, Maryland 20740, USA*
[3]*National Institute of Standards and Technology, Gaithersburg, Maryland 20899-8423, USA*
*joshua.pomeroy@nist.gov

An ultra-high vacuum (UHV) compatible Penning ion source for growing pure, highly enriched ^{28}Si epitaxial thin films is presented. Enriched ^{28}Si is a critical material for quantum information due to the elimination of nuclear spins. In some cases, the material must be grown by low temperature molecular beam epitaxy (MBE), e.g., scanning tunneling microscopy (STM) hydrogen lithography-based devices. Traditional high-purity physical vapor methods typically deliver a very small fraction of source material onto the target substrate, making the cost for use with highly enriched source materials very high. Thus, directed beam sources provide an efficient alternative. This UHV Penning source uses all metal or ceramic parts and a removable electromagnet to allow bake-out. The source gas is commercial (natural isotope abundance) silane gas (SiH_4), an inexpensive source material. High enrichment levels up to 99.99987 % (8.32×10^{-7} mol/mol ^{29}Si) and high chemical purity of 99.965 % are shown without post-processing. We present and discuss the discharge properties of this new source, the ion mass spectrum when coupled to our mass filter, and the secondary ion mass spectroscopy (SIMS) of the grown films.

I. INTRODUCTION

Isotopically enriched silicon based qubits that utilize electron and/or nuclear spins in quantum dots and/or donors are competitive candidates for quantum computation (or memory) due to very long coherence times [1], [2] and high gate fidelities [3],[4]. Compared to natural abundance silicon, the coherence times increase orders of magnitude when using isotopically enriched ^{28}Si as host material. Natural silicon contains ≈ 4.7 % ^{29}Si (nuclear I = ½), which causes random fluctuations and inhomogeneities in the background magnetic field and dramatically reduces the qubit coherence time. By reducing the ^{29}Si nuclear spin density to < 0.005 %, nuclear spin coherence times (T_{2n}) approaching an hour [5] and electron spin coherence times (T_{2e}) exceeding a second [6] have been reported in ^{28}Si using ^{31}P.

32 Despite the advantages of isotopically enriched ^{28}Si, the supply is very limited, due largely to the
33 extreme cost of enriching silicon. Perhaps the most highly enriched single crystal bulk ^{28}Si is
34 from the International Avogadro Project [7], which was produced using centrifuge enriched
35 gaseous silane and a long process chain resulting in zone refined, single crystal silicon with a
36 residual ^{29}Si isotope fraction of about 10^{-5} mol/mol [8]. The end goal in that case was to produce a
37 macroscopic artifact (≈1 kg) of enriched silicon for metrological purposes. Quantum information
38 applications do not require macroscopic quantities of ^{28}Si for each device, so an alternative, less
39 expensive strategy has been to grow epitaxial ^{28}Si layers on natural silicon substrates using
40 enriched silane gas. For example, chemical vapor deposition (CVD-grown) ^{28}Si epilayers grown
41 on 300 mm^2 substrates that is enriched to 99.992 % [9] . Remnants from other sources [10] of ^{28}Si
42 also exist, providing access for research efforts, typically with enrichments ≤ 99.9 % ^{28}Si,
43 including the float-zone grown samples from Keio University[11], CVD grown thin films at
44 Princeton University [12], solid-source molecular beam epitaxy (MBE) grown thin films at
45 Technical University of Munich (TUM) [13], ion beam method from Penning source based ion
46 implanter [14], etc. Generally, these isotopically enriched ^{28}Si materials are not extremely
47 enriched (≈ 99.9 % ^{28}Si), are of very limited quantity, and are not being replenished.

48 In addition to the general need for high quality ^{28}Si for quantum information sciences (QIS),
49 additional experiments are needed to determine the detailed relationship between enrichment and
50 quantum coherence. The exact value of enrichment required for QIS remains unknown. An ideal
51 solution would be to produce enriched silicon with many, different targeted enrichment levels
52 and systematically assess the performance (e.g., coherence time) of a test device. In theory work,
53 Witzel et al. predicted that with every order of magnitude increase in isotopic enrichment, the
54 coherence time will increase approximately an order of magnitude [15], but emerging experiments
55 have indicated performance with enrichment (0.08 % ^{29}Si) better than predicted, motivating
56 additional studies [2, 16]. Therefore, a source of ^{28}Si that can produce targeted enrichment levels
57 spanning a wide range would enable mapping of the decoherence time and provide specifications
58 for large-scale enriched silicon production.

59 We have previously reported on our ability to make very highly enriched ^{28}Si, where we used a
60 Penning ion source to ionize natural abundance SiH_4 gas, mass filtered the ions, decelerated to
61 hyperthermal energies, and deposited isotopically enriched ^{28}Si *in situ* [17],[18],[19]. Using this

62 method, enrichment of $^{28}Si > 99.99983$ % ($< 10^{-6}$ mol/mol ^{29}Si) was achieved. This is the highest
63 ^{28}Si enrichment known to be reported so far. However, the chemical purity of the silicon films
64 using this ion source was poor (98.47 %). Specifically, SIMS (secondary ion mass spectroscopy)
65 was used to determine the dominant chemical impurities of carbon (C), oxygen (O) and nitrogen
66 (N). Our prior system analysis assumed only background impurities in the growth chamber could
67 be incorporated, however, mass 28 u impurities mixed into the silane source gas in the inferior
68 vacuum region of the ion source were also transported ballistically (not just diffusively) along
69 with the silicon ion beam, due to their similar molecular mass. For example, N_2^+, CO^+ and other
70 mass 28 u ionized compounds such as $C_2H_4^+$ and CNH_2^+ can pass through our mass selector to
71 the sample since our mass resolution does not discriminate at that level (< 0.03 u).

72 Therefore, here we target the vacuum condition of the ion source area for improving the
73 chemical purity of our films. Our prior Penning source was not ultra-high vacuum (UHV)
74 compatible. It used rubber O-rings for vacuum seal and plastics for high voltage isolation with a
75 base pressure of $\approx 2.7 \times 10^{-6}$ Pa ($\approx 2 \times 10^{-8}$ Torr). Consequently, the ^{28}Si films grown using that
76 ion source had C concentrations in the range of 10^{20} cm^{-3}, and O and N concentrations in the
77 range of 10^{19} cm^{-3}, respectively. This impurity level is a problem for device fabrication (e.g.,
78 high quality oxide growth) and can potentially also act as a source of decoherence for qubits in
79 silicon [20, 21]. Therefore, a new UHV ion source is needed to eliminate residual gases in the ion
80 source and the chemical impurities in the ^{28}Si film.

81 As described above, the system with the newly designed UHV ion source must produce highly
82 enriched ^{28}Si ($< 10^{-6}$ mol/mol ^{29}Si) and improved chemical purity ($< 10^{18}$ cm^{-2} impurities). The
83 specific goals for this work are: 1) to reduce ionization source base pressure to $< 3 \times 10^{-8}$ Pa (≈ 2
84 $\times 10^{-10}$ Torr) to similarly increase the film chemical purity; 2) to identify the source's optimum
85 operating conditions for epitaxial thin film deposition; and 3) to enrich epitaxial ^{28}Si thin films to
86 $< 10^{-6}$ mol/mol ^{29}Si. In this paper, we present the details of our new ion source able to achieve
87 these goals, present the data and discuss these performance metrics.

88 **II. EXPERIMENTAL SETUP**

89 The design of our UHV ion source is described below. In addition to achieving ultra-high
90 vacuum, this UHV ion source must also be compatible with the existing ion transport, mass filter
91 and deposition system. The details of the associated system can be found elsewhere [18], however,

92 a brief description is presented here to assist understanding. The enriched silicon system consists
93 of four subsystems: the gas handling, the ionization source, ion transport, and the deposition
94 chamber, which is additionally coupled to a load lock and a scanning tunneling microscope
95 (STM) chamber that will not otherwise be discussed here. The ion source is a Penning-type ion
96 source [22], which has a cylindrical anode and cathodes at each end that creates an axial confining
97 potential well. The ion's radial confinement is provided by an axial magnetic field from an
98 electromagnet, which also helps focus ions for extraction. During the discharge, a plasma is
99 formed by accelerating electrons from the cathodes that ionize the gas molecules. SiH_4 is used in
100 this case, although Ar and Ne have also been used for diagnostics. Ions are extracted using an
101 extraction cusp adjacent to one end of the source and transmitted into a system of electrostatic
102 lenses. Since we require hyperthermal energy ions (< 50 eV kinetic energy) that are susceptible
103 to Coulomb repulsion (space charge) effects [23], the transport system is typically operated at -4
104 kV (i.e., ions are accelerated to > 4 keV while transiting the lenses and mass filter) and
105 decelerated before deposition. As a result, high voltage isolation between the ion source and the
106 rest of the systems (transport and gas inlet) is required. In the prior ion source, a plastic transition
107 plate was used as electric isolation and was one of the major causes of poor vacuum. In the new
108 design, we use an 8" CF reducer nipple with ceramic neck to mate the ion source to the transport
109 system and use ceramic standoffs for the gas inlet, as shown in Fig.1.

110 Apart from the compatibility with the existing system, several other factors constrain the design
111 of this UHV ion source. First, all components need to be UHV ($< 1.33 \times 10^{-7}$ Pa or 10^{-9} Torr)
112 compatible and bakeable (> 150 ºC), including the gas injection. Therefore, all tubes from the
113 SiH_4 gas bottle to the ion source feedthrough use vacuum coupling radiation (VCR) fittings to
114 prevent air (C, O, N rich) from leaking into the gas line. Second, all plastics components such as
115 polytetrafluoroethylene (PTFE) and nylon are replaced with ceramics. Plastics can contribute
116 fluorine and chlorine compounds, as well as lighter gases, and present problems when the ion
117 source becomes hot during baking. Third, the prior ion source's electromagnet was buried inside
118 the housing without efficient cooling. Heating of the electromagnet caused outgassing and source
119 instability, the wire insulation commonly failed, and baking was not possible. In the new design,
120 the magnet is a separate component outside the vacuum system, water-cooled and removable for
121 baking. Furthermore, to ease replacement of the anode and cathodes, the core of the ion source
122 can be easily taken in and out without disturbing the magnet or other elements. Finally, the new

123 ion source is designed to be compact and easy to maintain, using mostly simple or commercial
124 parts.

125 A schematic of the UHV Penning ion source is shown in Fig.1 and discussed in detail below.
126 Our design goal was to keep the ion source dimensions as compact as possible and fully
127 supported by the 70 mm CF base flange, while also having > 5 kV electrical isolation between
128 the anode and the cathodes. The ion source is shown in Fig.1 with dimensions and geometry
129 correct according to the scale bar. The ion source's plasma region has three main consumable
130 components shown as dark red: the anode, cathode and anti-cathode inserts. The distance
131 between the cathodes and the anode is based on Ref. [24], where the performance of the gas
132 discharge has been optimized. The anode, cathode and anti-cathode supports are 304 stainless
133 steel (SS). The cathode inserts are constantly eroded by ions during plasma discharge and this
134 design allows the anode and cathode inserts to be replaced easily, minimizing the maintenance
135 steps and time. The lifetime of the cathodes depends on material type, gas source and energy of
136 the impact, but typical insert lifetimes are about 30 h.

137 For the purpose of hyperthermal (5 eV to 100 eV) ^{28}Si epitaxial thin film growth, the plasma
138 potential and the final energy of the ions are approximately set by the anode voltage [18], which is
139 typically set to be around 50 V. The hyperthermal energy range allows atoms to land softly onto
140 the substrate during deposition, optimizing the ^{28}Si island density and crystalline quality without
141 introducing point defects[18].

142 The high voltage feedthroughs and the gas inlet are also shown on the base flange at right. The
143 anode and cathode supports are connected by small copper wires that pass through thin insulating
144 tubes to the feedthroughs and are fixed with vented screws (to prevent virtual leaks). Ceramic
145 rings and top hat washers are inserted to provide electrical isolation between cathodes and anode,
146 which typically have a 3 kV potential difference, and to maintain good geometric alignment. The
147 main body (vacuum wall) is designed to be at the cathode potential (copper standoffs) or at a
148 different potential, e.g., earth ground (ceramic standoffs—shown). For example, using ceramic
149 standoffs allows the ion source body to be grounded so that a mass flow controller can be
150 installed to provide precise control of the gas flow. Under some circumstances, the plasma power
151 can substantially heat the central components leading to high voltage breakdown, which can be
152 better mitigated with the copper standoffs that conduct heat away efficiently.

153 **III. RESULTS AND DISCUSSIONS**

154 The discharge properties of this UHV ion source using SiH_4 gas are studied to determine the
155 optimum operation conditions. The arc (plasma) current and the total ion beam current extracted
156 from the ion source are affected by the ion density and the electron temperature of the discharge,
157 and those quantities are influenced by the arc voltage, flow rate and source magnetic field [24]. In
158 Fig.2, the total $^{28}Si^{+}$ ion current and arc current are shown as functions of these three parameters.
159 The measurements were done by first maximizing the ion current while changing source
160 magnetic field and flow rate at -2.7 kV arc voltage. These values of magnetic field and flow rate
161 are then marked as optimum values H_{opt} and F_{opt} in Fig.2. Then, each of the three parameters is
162 uniaxially varied while the other two are kept constant at their optimum values.

163 The ion and arc current dependence on arc voltage is shown in Fig.2(a). The discharge begins at
164 around -1.7 kV and the ion current increases monotonically with the arc voltage up to a first
165 maximum at -2.7 kV, and then shows weak structure suggestive of higher order plasma modes at
166 -3.4 kV and -3.8 kV. The arc current shows a similar trend but reaches a maximum at -2.4 kV
167 and has weaker mode structure. In Fig.2(b), the ion current versus source magnetic field is shown
168 while keeping the arc voltage at -2.7 kV and the gas flow at -0.02 sccm. The plasma ignites at
169 about 0.6 T and the total ion current increases rapidly reaching a maximum at 0.67 T. Here the
170 mode structure is more pronounced with two other ion current maxima appearing at 0.77 T and
171 0.86 T. The arc current again shows a similar trend to the ion current, where three somewhat
172 weaker, corresponding maxima are observed. The variation of the ion current vs. the flow rate
173 while keeping the arc voltage at -2.7 kV and the magnetic field at 0.77 T is shown in Fig.2(c).
174 Unlike in arc voltage and source magnetic field, the ion current vs. flow rate shows a large peak
175 at 0.02 sccm and a softer, broader peak at 0.11 sccm. The arc currents increase monotonically
176 after ignition over the entire range studied. The optimum operating condition for ^{28}Si deposition
177 using SiH_4 gas is therefore at -2.7 kV arc voltage, 0.77 T source magnetic field and 0.02 sccm
178 (1.87×10^{-4} Pa or 1.4×10^{-6} Torr) flow rate. These values closely match those of the previous ion
179 source on which this source was based [24].

180 Having discussed the plasma performance of the ion source, we now move on to evaluating the
181 improvements in gas cleanliness and efficacy for silicon enrichment that motivate this effort. To
182 effectively enrich the silicon, once the ion source is coupled to the beamline [18], the transmitted

183 silicon ions must have trajectories well separated from each other when sweeping the magnetic
184 field of the ion mass separator in the beamline. This allows one mass to be selected by the
185 separator aperture while rejecting other masses. The mass spectra of the silicon ion beam taken
186 with the prior and UHV ions sources are compared and shown in Fig. 3(a). The ion mass
187 spectrum is collected using a second, custom aperture plate on the sample stage to monitor the
188 ion current while scanning the magnetic field of the mass analyzer. Six singly charged SiH_4
189 related peaks are shown. The first peak at mass 28 u corresponds to $^{28}Si^{+}$ ions, while the rest of
190 the peaks result from a combination of isotopes and hydrides due to the incomplete cracking of
191 SiH_4 gas molecules. In ion beam deposition, the enrichment is dominated by the mass separation
192 between mass 28 u and 29 u peaks (See ref. [17] for detailed analysis of mass selectivity). The
193 UHV ion source's similar peak shape and separation compared to the prior source indicate good
194 mass selectivity for enrichment, and similar current suggests a similar growth efficiency with this
195 ion source. Typically, we use a deposition rate of 0.99 nm/min and the ion source is stable
196 throughout the deposition (usually 6 h to 8 h). Higher growth rate might be achieved by using
197 different plasma modes (e.g. higher flow rate), but generally results in shorter cathode lifetime
198 and larger surface roughness of the deposited film.

199 The enrichment expected from the mass spectrum is verified in Fig.3(b) using SIMS (secondary
200 ion mass spectroscopy) to profile the isotopic fraction of ^{28}Si, ^{29}Si and ^{30}Si of the deposited ^{28}Si
201 film grown using this UHV ion source. The SIMS measurement was taken near the center part of
202 the enriched silicon film, which is usually the thickest. The residual isotope fraction of ^{29}Si is
203 shown as squares with an average value of $8.32(80) \times 10^{-7}$ mol/mol in the film and ^{30}Si is shown
204 as triangles with an average value of $4.91(65) \times 10^{-7}$ mol/mol. The ^{28}Si total enrichment for this
205 sample is 99.99987(3) %. The enrichment level can vary some from run to run, but comparing
206 several samples deposited using the prior ion source with samples from this ion source, we
207 conclude that the ^{28}Si enrichment is maintained with this UHV ion source.

208 Since the growth chamber pressure is typically maintained at 6.7×10^{-9} Pa (5×10^{-11} Torr), the
209 background gas composition in the ion source was the leading contributor to film contamination
210 in the prior source and the primary motivation for building a UHV ion source. The baseline
211 pressure as measured with an ion gauge (uncertainty of 10 % to 20 %) has been improved by a
212 factor of a hundred in this UHV ion source compared to the prior ion source, now reaching 2.7 $\times$

213 10^{-8} Pa (2×10^{-10} Torr). The partial pressures of various gas components as measured by a
214 residual gas analysis (RGA) in the prior and UHV ion sources are shown in Fig.4(a) and Table I.
215 These show the qualitative improvement in vacuum conditions and chemical compositions and
216 confirm that the impurities contributed from the ion source vacuum have been reduced by a
217 factor of 100.

218 A SIMS depth profile showing the chemical impurity concentrations for C, N, O, F and Cl in a
219 ^{28}Si thin film deposited using this UHV ion source is shown in Fig.4(b). The average
220 concentration level for carbon is $9.5(8) \times 10^{18}$ cm^{-3}; nitrogen is $5.5(5) \times 10^{18}$ cm^{-3} and oxygen is
221 $2.1(2) \times 10^{18}$ cm^{-3} between 30 nm and 235 nm. As compared to the prior ion source, the total
222 chemical purity of the ^{28}Si film has been improved from ≈ 98.5 % to 99.965(2) %. From previous
223 SIMS measurement (not shown), we found that the ^{12}C concentration in the film is roughly 400
224 times higher than ^{13}C. This means that the ^{12}C is also enriched (> 98.9 %) in the ion beam
225 process and the ^{13}C concentration is approximately 3×10^{16} cm^{-3}. Similarly, the ^{15}N
226 concentration is $< 2 \times 10^{16}$ cm^{-3}. Therefore, at this contamination level, the dominating factor for
227 nuclear spin bath is still expected to be ^{29}Si, plus some contributions from ^{13}C and ^{15}N as well.
228 Future improvement in chemical purity is needed to reduce the effects from ^{13}C and ^{15}N.

229 Despite the substantial improvement in chemical purity (43x), we found the improvement was
230 not fully correlated to the vacuum improvement (100x). This indicates that at this concentration
231 level, the vacuum condition of the ion source is not the only limiting factor that affects the
232 chemical purity of the ^{28}Si film. We also found that the impurity concentrations are not
233 correlated to the growth rate, indicating the origin of the impurities is from the ion source
234 chamber instead of the growth chamber. Therefore, the cleanliness of the silane gas system
235 (silane is highly reactive), impurity ions sputtering from the cathodes and anode materials and
236 chemical compounds formed in the ion source plasma may be contributing factors. Further study
237 is needed to fully explore the origin of the contaminations in the film and to seek additional
238 purity improvements. Possible solutions may include reaching better ion source base pressure,
239 using silane gas purifier to purify the gas line, and post-annealing at 950 °C in UHV (preliminary
240 work shows that the N concentration can be reduced to low 10^{17} cm^{-3} after annealing), etc.
241 Electronic and quantum devices will then be developed to determine the deleterious impacts of
242 the residual contaminants to relevant device performance.

243 **IV. Conclusion**

244 In this paper, we present the design, experimental implementation and performance of a UHV
245 ion source system. The discharge properties based on arc voltage, source magnetic field and flow
246 rate have been studied and optimized for ^{28}Si. The performance of the UHV ion source for
247 enriched silicon deposition is demonstrated through the ion mass spectrum and SIMS
248 measurements of an enriched film. We show that the isotopically enriched ^{28}Si thin film
249 deposited has high enrichment level of 99.99987(3) % ($(8.32 \pm 0.80) \times 10^{-7}$ mol/mol ^{29}Si) and
250 chemical purity of 99.965(2) %, a substantial improvement over the prior ion source while
251 maintaining the ability for highest enrichment among all methods reported. We believe this is an
252 important step forward to produce high quality ^{28}Si that is suitable for quantum information
253 studies.

254

255

256 # Tables

257 TABLE I. Partial pressures of key gas contaminants relevant to silicon thin film purity as measured
258 by residual gas analysis (RGA). Qualitatively the uncertainty is in the range of 10 % to 20 %.

Impurity	*Mass (u)*	*Pressure in prior ion source (Pa)*	*Pressure in UHV ion source (Pa)*
H_2O	18	$> 1.4 \times 10^{-7}$	6.1×10^{-10}
N_2	28	7.3×10^{-8}	1.1×10^{-9}
O_2	32	6.3×10^{-8}	2.8×10^{-11}
CO_2	44	6.5×10^{-8}	3.5×10^{-10}

259

260

Figures

Fig.1. Simplified, cross sectional schematic diagram of the UHV ion source sliced along the axis – most parts are cylindrically symmetric. Insulating parts are shown in off-white. Consumable parts are dark red. The vacuum housing is unhatched with the stainless steel components shown in gray. The electromagnet solenoid is shown shaded brown and cross-hatched above and below the ion source insert. Source gas enters from the right, and ions are extracted to the left, where a system of electrostatic optics transports them downstream (not shown).

272 Fig.2 (a)

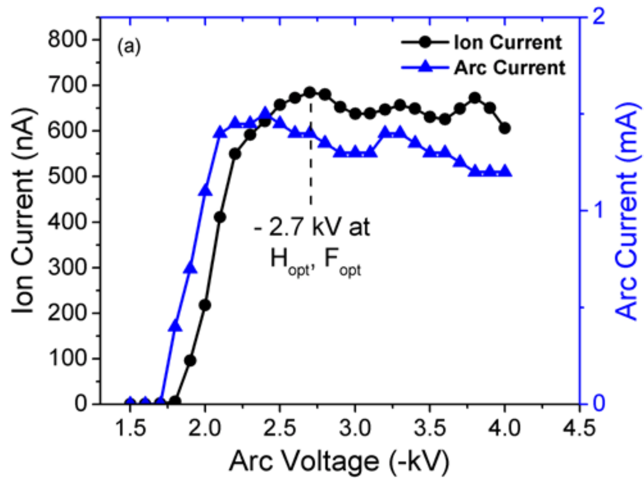

273

274 Fig.2 (b)

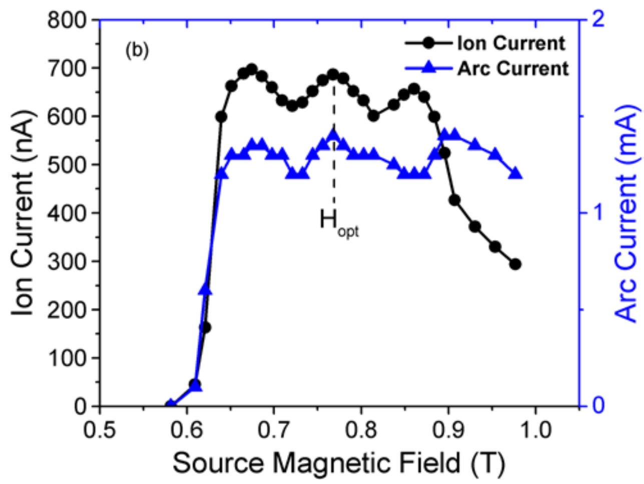

275

276 Fig.2 (c)

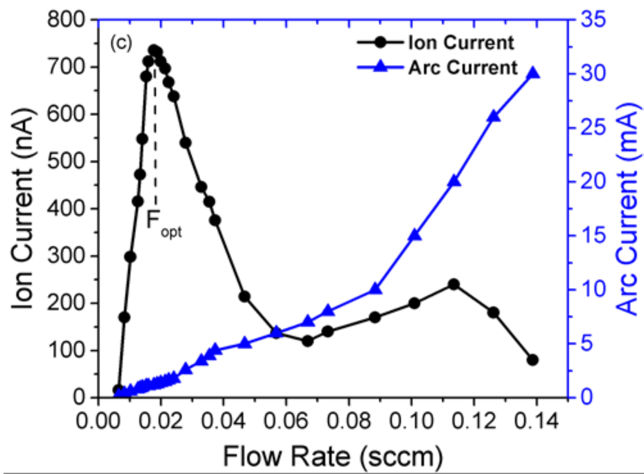

277

278 Fig.2. ^{28}Si ion current (black) and discharge current (blue) characteristics: (a) as a function of arc
279 voltage; (b) as a function of source magnetic field, and (c) as a function of SiH_4 flow rate. The
280 measurement uncertainties are ± 1 nA for ion current and ± 0.2 mA for arc current, respectively.

281

282 Fig.3 (a)

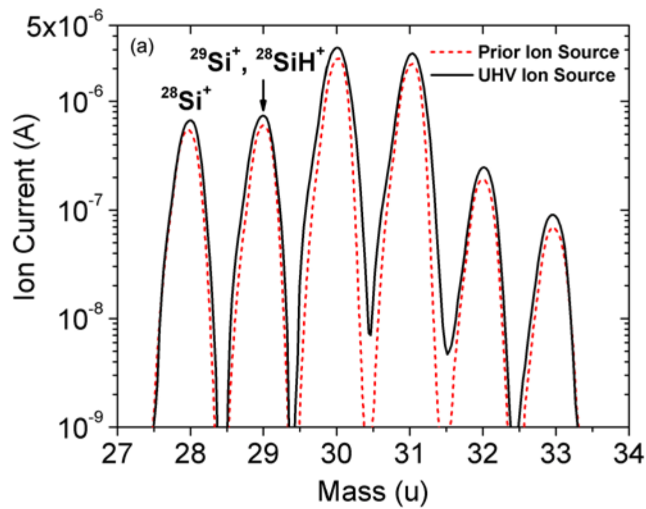

283

284 Fig.3 (b)

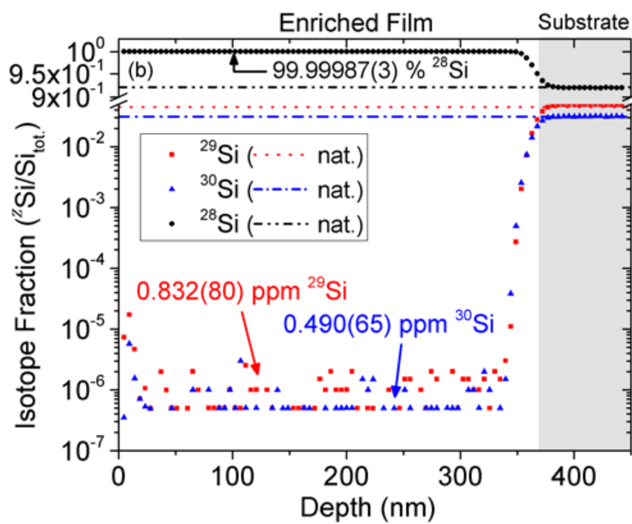

285

286 Fig.3. (a) The ion beam mass spectra of the prior (red dashed) and new (solid black) UHV ion
287 source are shown for comparison. The ion current after passing through the mass selecting
288 magnet shows six peaks, which consist mostly of $^{28}Si^+$ ions at 28 u and other isotopes combined
289 with hydrides at higher masses. The peak shapes and isotope separation between 28 u and 29 u
290 indicate similar enrichment capability. (b) A SIMS depth profile of ^{28}Si thin film shows the
291 isotope fractions of ^{28}Si, ^{29}Si and ^{30}Si using the UHV ion source, confirming excellent
292 enrichment with an average of 99.99987(3) %.

293 Fig.4 (a)

294

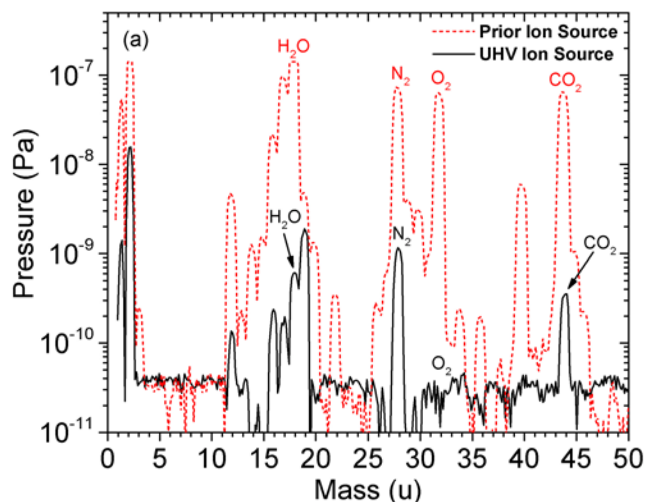

295 Fig.4(b)

296

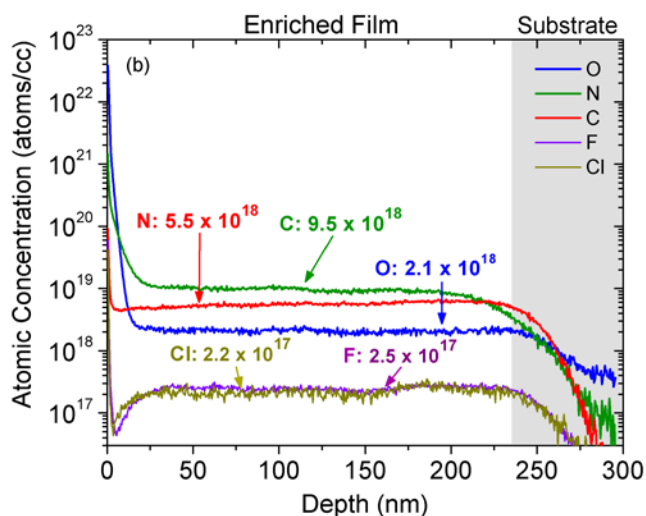

297 Fig.4. (a) Residual gas analysis (RGA) demonstrating the comparison in background gas density
298 between the two ion sources. The red curve in (a) is the prior ion source with base pressure $2.7 \times$
299 10^{-6} Pa (2×10^{-8} Torr) and the black curve is the UHV ion source with base pressure 2.7×10^{-8}
300 Pa (2×10^{-10} Torr). Major peaks are labeled with the dominant gases. (b) A SIMS depth profile
301 of the residual chemical impurities in a ^{28}Si thin film deposited using the UHV ion source. The
302 estimated chemical purity of this sample is 99.965(2) %.

303

304 **REFERENCES**

305 1. Veldhorst, M., et al., *An addressable quantum dot qubit with fault-tolerant control-fidelity.*
306 Nature Nanotechnology, 2014. **9**(12): p. 981.

307 2. Muhonen, J.T., et al., *Storing quantum information for 30 seconds in a nanoelectronic device.*
308 Nature Nanotechnology, 2014. **9**(12): p. 986.
309 3. Yoneda, J., et al., *A quantum-dot spin qubit with coherence limited by charge noise and fidelity*
310 *higher than 99.9%.* Nature Nanotechnology, 2018. **13**(2): p. 102.
311 4. Veldhorst, M., et al., *A two-qubit logic gate in silicon.* Nature, 2015. **526**(7573): p. 410.
312 5. Saeedi, K., et al., *Room-Temperature Quantum Bit Storage Exceeding 39 Minutes Using Ionized*
313 *Donors in Silicon-28.* Science, 2013. **342**(6160): p. 830-833.
314 6. Tyryshkin, A.M., et al., *Electron spin coherence exceeding seconds in high-purity silicon.* Nature
315 Materials, 2012. **11**(2): p. 143.
316 7. Becker, P., et al., *Enrichment of silicon for a better kilogram.* Physica Status Solidi a-Applications
317 and Materials Science, 2010. **207**(1): p. 49-66.
318 8. Abrosimov, N.V., et al., *A new generation of 99.999% enriched (2)8(S)i single crystals for the*
319 *determination of Avogadro's constant.* Metrologia, 2017. **54**(4): p. 599-609.
320 9. Mazzocchi, V., et al., *99.992% ^{28}Si CVD-grown epilayer on 300 mm substrates for large scale*
321 *integration of silicon spin qubits.* Journal of Crystal Growth, 2019. **509**: p. 1-7.
322 10. Itoh, K.M. and H. Watanabe, *Isotope engineering of silicon and diamond for quantum computing*
323 *and sensing applications.* MRS Communications, 2014. **4**(4): p. 143-157.
324 11. Takyu, K., et al., *Growth and characterization of the isotopically enriched Si-28 bulk single crystal.*
325 Japanese Journal of Applied Physics, 1999. **38**(12b): p. L1493.
326 12. Li, J.Y., et al., *Extremely high electron mobility in isotopically-enriched Si-28 two-dimensional*
327 *electron gases grown by chemical vapor deposition.* Applied Physics Letters, 2013. **103**(16): p.
328 162105.
329 13. Sailer, J., et al., *A Schottky top-gated two-dimensional electron system in a nuclear spin free*
330 *Si/SiGe heterostructure.* Physica Status Solidi-Rapid Research Letters, 2009. **3**(2-3): p. 61-63.
331 14. Fiedler, H., et al., *$^{28}Si^{+}$ ion beams from Penning ion source based implanter systems for near-*
332 *surface isotopic purification of silicon.* Review of Scientific Instruments, 2018. **89**(12): p. 123305.
333 15. Witzel, W.M., et al., *Electron Spin Decoherence in Isotope-Enriched Silicon.* Physical Review
334 Letters, 2010. **105**(18): p. 187602.
335 16. Tracy, L.A., et al., *Single shot spin readout using a cryogenic high-electron-mobility transistor*
336 *amplifier at sub-Kelvin temperatures.* Applied Physics Letters, 2016. **108**(6): p. 063101.
337 17. Dwyer, K.J., et al., *Enriching Si-28 beyond 99.9998% for semiconductor quantum computing.*
338 Journal of Physics D-Applied Physics, 2014. **47**(34): p. 345105.
339 18. Pomeroy, J.M., et al., *Hyperthermal ion beam system optimized for studying the effects of kinetic*
340 *energy on thin-film growth.* Review of Scientific Instruments, 2002. **73**(11): p. 3846-3852.
341 19. Dwyer, K.J., et al., *Temperature-dependent Si-29 incorporation during deposition of highly*
342 *enriched Si-28 films.* Physical Review Materials, 2017. **1**(6): p. 064603.
343 20. Tyryshkin, A.M., et al., *Coherence of spin qubits in silicon.* Journal of Physics-Condensed Matter,
344 2006. **18**(21): p. S783.
345 21. Culcer, D. and N.M. Zimmerman, *Dephasing of Si singlet-triplet qubits due to charge and spin*
346 *defects.* Applied Physics Letters, 2013. **102**(23): p. 232108.
347 22. Penning, F.M., *A new manometer for low gas pressures especially between 10(-3) and 10(-5)*
348 *mm.* Physica, 1937. **4**: p. 71-5.
349 23. Pierce, J.R., *Theory and design of electron beams*. 2nd ed. The Bell Telephone Laboratories
350 series. 1954, New York,: Van Nostrand.
351 24. Baumann, H. and K. Bethge, *Pig Ion-Source with End Extraction for Multiply Charged Ions.*
352 Nuclear Instruments & Methods, 1974. **122**(3): p. 517-525.

353